Chemical Abundance Analysis of the Symbiotic Red Giants

Cezary Gałan[1], Joanna Mikołajewska[1], and Kenneth H. Hinkle[2]

[1]*N. Copernicus Astronomical Center, Bartycka 18, PL-00-716 Warsaw, Poland*

[2]*National Optical Astronomy Observatory, P.O. Box 26732, Tucson, AZ 85726, USA*

Abstract. The study of symbiotic stars - the long period, interacting binary systems - composed of red giant donor and a hot, compact companion is important for our understanding of binary stellar evolution in systems where mass loss or transfer take place involving RGB/AGB stars. The elemental abundances of symbiotic giants can track the mass exchange history and can determine their parent stellar population. However, the number of these objects with fairly well determined photospheric composition is insufficient for statistical considerations. Here we present the detailed chemical abundance analysis obtained for the first time for 14 M-type symbiotic giants. The analysis is based on the high resolution (R $\sim$ 50000), high S/N $\sim$ 100, near-IR spectra (at H- and K-band regions) obtained with Phoenix/Gemini South spectrometer. Spectrum synthesis employing standard LTE analysis and atmosphere models was used to obtain photospheric abundances of CNO and elements around the iron peak (Sc, Ti, Fe, and Ni). Our analysis reveals mostly slightly sub-solar or near-solar metallicities. We obtained significantly subsolar metallicities for RW Hya, RT Ser, and Hen 3-1213 and slightly super-solar metallicity in V455 Sco. The very low $^{12}C/^{13}C$ isotopic ratios, $\sim$6-11, and significant enrichment in nitrogen ^{14}N isotope in almost all giants in our sample indicate that they have experienced the first dredge-up.

1. Introduction

Symbiotic stars are long period binary systems, composed of two evolved and strongly interacting stars: a red giant donor and a hot and luminous white dwarf companion (occasionally a neutron star) surrounded by an ionized nebula. Phenomena connected with mass loss and mass exchange between two evolutionary advanced stars make symbiotic systems particularly useful for studying the late stages of binary evolution. The elemental abundances of symbiotic giants determines the stellar population and can track the mass exchange history.

Reliable measurements of photospheric compositions exist for only a few symbiotic systems with normal red giants and about a dozen of so called yellow symbiotic systems (Mikołajewska et al. 2014 and referenced therein) – to small a sample for statistical considerations. To improve this situation we have undertaken a research program of detailed chemical composition analysis on >30 symbiotic systems. Here we present the results obtained for 14 objects listed in the Table .1.

2. Observations and data reduction

High-resolution ($R \sim 50000$), high S/N (≥ 100) near-IR spectra were observed with the Phoenix cryogenic echelle spectrometer on the 8 m Gemini South telescope in 2003–2006. The spectra cover narrow wavelength ranges (∼100Å) located in the H and K photometric bands at mean wavelengths 1.563, 2.225, and 2.361 μm (hereafter H, K, and $K_{\rm r}$-band spectra, respectively). The H-band spectra contain molecular CO and OH lines, K-band spectra CN lines, and in both these ranges numerous, strong atomic lines are present. These lines were used to determine abundances of CNO and elements around iron peak: Sc, Ti, Fe, Ni. The $K_{\rm r}$-band spectra are dominated by strong CO features that enable measurement of the ^{12}C/^{13}C isotopic ratio. The spectra were extracted and wavelength calibrated using standard reduction techniques Joyce (1992) and all were heliocentric corrected. In all cases telluric lines were either not present or were removed by reference to a hot standard star. The Gaussian instrumental profile is in all cases about 6 km s^{-1} FWHM corresponding to instrumental profiles of 0.31, 0.44, and 0.47 Å in the case of the H-band, K-band, and $K_{\rm r}$-band spectra, respectively.

3. Methods

Abundance analyses were performed by fitting synthetic spectra to observed ones with a method similar to that used for CH Cyg (Schmidt et al. 2006). Standard *LTE* analysis and *MARCS* model atmospheres (Gustafsson et al. 2008) were used for the spectral synthesis. The code *WIDMO* developed by M.R. Schmidt (Schmidt et al. 2006) was used to calculate synthetic spectra and the simplex algorithm (Brandt 1998) for the χ^2 minimization. The atomic data were taken from the *VALD* database (Kupka et al. 1999) in the case of K- and $K_{\rm r}$-band regions and from the list given by Melendez & Barbuy (1999) for the H-band region. For the molecular lines we used the line lists published by Goorvitch (1994) (CO) and from CD-ROMs of Kurucz (^{12}CN and OH).

The input effective temperatures $T_{\rm eff}$ were estimated from the known spectral types (Mürset & Schmidt 1999) by adopting two calibrations (Richichi et al. 1999; van Belle et al. 1999). The infrared intrinsic colors derived from the 2MASS (Phillips 2007) magnitudes, and color excesses (Schlafly et al. 2011), combined with the $T_{\rm eff}$–log g–*color* relation for late-type giants (Kucinskas et al. 2005), resulted in surface gravities and effective temperatures that are in good agreement with those from the spectral types. The adopted stellar parameters ($T_{\rm eff}$ and log g) are presented in Table .1. The macroturbulence velocity $\zeta_{\rm t}$ was set at 3 km/s, a value typical for the cool red giants (e.g. Fekel et al. 2003).

The radial velocities for individual spectra were obtained with a cross-correlation technique (Carlberg et al. 2011) with synthetic spectra used as the template. The rotational

Table .1: Stellar parameters, $T_{\rm eff}$ and $\log g$ estimated from spectral types and $T_{\rm eff}$-$\log g$-*color* relation.

Object	**Sp.T.**	$\mathbf{T_{eff}}$	$\mathbf{J-K}$	$\mathbf{(J-K)_0}$	$\mathbf{T_{eff}}^{\star}$	$\mathbf{\log g}^{\star}$	**Ref.**
	[1]	[2,3]	[4,5]		[6]	[6]	
RW Hya	M2	3670	1.15	1.1	3700	0.5	[7]
SY Mus	M5	3360	1.40	1.2	3400	0.5	[7]
BX Mon	M5	3360	1.37	1.3	3400	0.0	[8]
AE Ara	M5.5	3310	1.36	1.25	3300	0.0	[8]
KX TrA	M6	3250	1.39	1.3	3300	0.0	[8]
CL Sco	M5	3360	1.29	1.15	3400	0.5	[8]
V694 Mon	M6	3250	1.42	1.3	3300	0.0	‡
CD-36 8436	M5.5	3310	1.27	1.25	3300	0.0	‡
WRAY 16-202	M6	3250	2.09	...	3300	0.0	‡
Hen 2-247	M6	3250	1.61	1.35	3300	0.0	‡
AS 270	M5.5	3310	1.75	1.05	3300	0.0	‡
RT Ser	M6	3250	1.56	1.3	3300	0.0	‡
V455 Sco	M6.5	3190	1.62	1.25	3200	0.0	‡
Hen 3-1213	$\leq$K4	$\leq$4100	1.37	0.9	4100	1.5	‡

$\star$ adopted; ‡ this work; [1] Mürset & Schmidt (1999); [2] Richichi et al. (1999); [3] van Belle et al. (1999); [4] Phillips (2007); [5] Bessell & Brett (1989); [5] Kucinskas et al. (2005); [6] Mikołajewska et al. (2014); [7] Gałan et al. (2014)

velocities were estimated via direct measurement of the FWHM of six relatively strong, unblended atomic lines (Ti I, Fe I, Sc I) present in the K-band region (Fekel et al. 2003). The resulting values of the radial and rotational velocities were set as a fixed parameters in our solutions.

To carry out the abundance solution, solar composition (Asplund et al. 2009) abundances of CNO and iron peak elements were adjusted by fitting by eye, iteratively, OH, CO, CN and atomic lines. Next the initial grid of the $n+1$, n dimensional sets of free parameters – so called simplex needed for the simplex algorithm – was prepared. Minimization was performed with nine different simplexes that were used with different microturbulent velocities ($\xi_{\rm t}$) sampled in the range 1.2–2.6 km/s to obtain an optimal fit to H- and K-band spectra. For the six objects for which $K_{\rm r}$-band spectra were available, after we found the sets of parameters giving the best fit to the H- and K-band spectra, we applied these abundances to the $K_{\rm r}$-band spectrum as a fixed parameter and we searched for ^{12}C/^{13}C isotopic ratio. After obtaining the optimal fit, we made a reconciliation of ^{12}C and ^{12}C/^{13}C within several iterations.

Table .2: Calculated abundances, $^{12}C/^{13}C$ isotopic ratios, microturbulences ξ_t, and estimated formal errors.

Object	A(C)	A(N)	A(O)	A(Sc)	A(Ti)	A(Fe)	A(Ni)	$^{12}C/^{13}C$	ξ_t
RW Hya	7.53	7.46	8.17	2.71	4.49	6.74	5.63	6	1.8
SY Mus	8.17	8.11	8.66	3.97	5.12	7.42	6.37	10	2.0
BX Mon	7.79	7.89	8.37	3.82	4.96	7.16	6.18	8	1.8
AE Ara	8.10	8.15	8.64	4.53	5.40	7.41	6.28	...	1.7
KX TrA	8.03	8.04	8.66	4.02	5.08	7.17	6.21	...	1.9
CL Sco	8.02	8.14	8.61	3.47	4.93	7.21	6.23	...	1.9
V694 Mon	8.10	7.85	8.43	3.19	4.83	7.11	5.92	26	2.0
CD-36 8436	7.76	7.91	8.37	3.66	4.81	7.12	6.13	8	2.0
WRAY 16-202	8.05	8.27	8.63	4.22	5.25	7.52	6.30	11	2.1
Hen 2-247	8.22	8.51	8.84	4.53	5.61	7.62	6.40	...	2.0
AS 270	8.01	8.00	8.47	4.02	5.09	7.34	6.16	...	1.7
RT Ser	8.01	7.93	8.36*	3.88	4.89	6.96	...	...	2*
V455 Sco	8.47	8.90	9.23	4.42	5.50	7.80	6.49	...	1.9
Hen 3-1213	7.97	7.69	8.84	3.29	4.92	6.71	5.69	...	2.1
Formal Errors	**< 0.05**	**< 0.05**	**< 0.05**	**∼ 0.05**	**∼ 0.1**	**< 0.05**	**∼ 0.05**	**∼ 2**	**∼ 0.2**
CH Cyg‡	8.37	8.08	8.76	...	5.24	7.50	6.65	18	2.2
Sun$^\odot$	8.43	7.83	8.69	3.15	4.95	7.50	6.22	...	...

$\star$ adopted; ‡ from Schmidt et al. (2006);
$\odot$ Solar composition by Asplund et al. (2009)

4. Results and discussion

The final derived abundances for CNO elements and atomic lines (Ti I, Fe I, Ni I, Sc I) on the scale $A(X) = \log \epsilon(X) = logN(X)N(H)^{-1} + 12.0$ are summarized in the Table .2 together with obtained microturbulent velocities, $^{12}C/^{13}C$ isotopic ratios and estimations of the formal errors. Solar (Asplund et al. 2009) and CH Cyg (Schmidt et al. 2006) abundances are shown for comparison. Examples of synthetic fits to the H-, K-, and K_r-band spectra of BX Mon are shown in Figure .1.

The elemental abundances of the symbiotic giants can be used to address their evolutionary status and to associate them with stellar populations of the Milky Way. In particular, the carbon and nitrogen abundances are very good monitors of dredge-up on the red giant branch, provided that only the CN cycle has operated significantly in the dredged material. In such a case, the total number of C+N nuclei should be conserved while ^{12}C will be converted to ^{14}N. Figure .2 shows the nitrogen and carbon abundances for the symbiotic sample thus far analyzed. All symbiotic giants fall into ^{14}N-enhanced zone providing a very strong indication that they have experienced the first dredge-up which is also confirmed by the low carbon isotopic ratios whenever their estimate was possible (Table .2). Note that V694 Mon

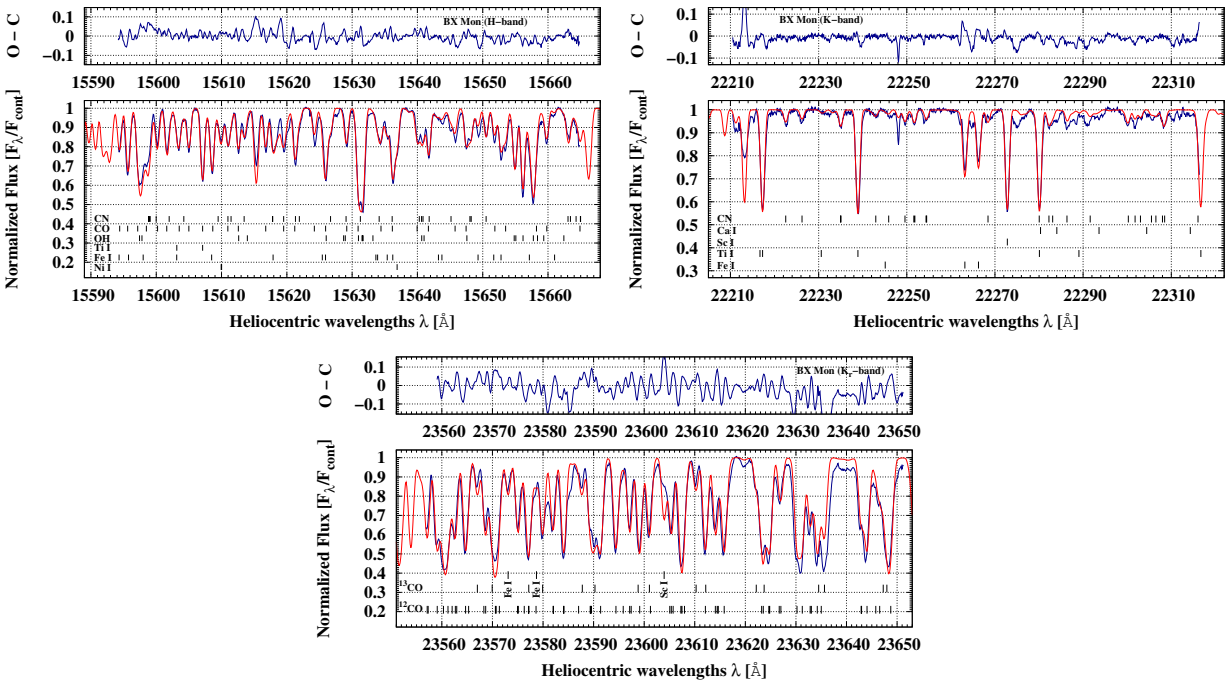

Figure .1: The spectra of BX Mon observed in February 2003 in the H-band (top–left), in April 2003 in the K-band (top–right), and in April 2006 in the K_r-band (bottom), compared with synthetic spectra (red lines) calculated using the final abundances, and $^{12}C/^{13}C$ isotopic ratio (Table .2).

and CH Cyg, which have somewhat higher $^{12}C/^{13}C$ isotopic ratios are less elevated in this plane.

Assuming, that oxygen and iron, and other elemental abundances, roughly, represent the original values with which stars were born these abundances can identify their parent Galactic population. The ratio of α-elements (e.g. oxygen) to iron is of particular importance because the α-elements originate mostly from massive stars and type II supernovae, and they are produced over relatively short timescales whereas Fe is most effectively produced in type Ia supernovae over much longer timescales. Thus, differences in contamination by both kinds of supernovae lead to significantly different trends for particular populations, and their clear separation in the [O/Fe] vs. [Fe/H] plane what is shown in Figure .3 where the members of four Galactic populations are taken from number of studies (Gałan et al. 2014) and after scaling to the solar composition (Asplund et al. 2009).

Our analysis reveals in most cases a slightly subsolar or solar metallicities (Table .3). In the case of RT Ser, RW Hya, and Hen 3-1213 we obtained significantly subsolar metallicities ([Fe/H] $\sim 0.5 - -0.8$), wherease one object – V455 Sco – shows a slightly supersolar metallicity ([Fe/H] $\sim +0.3$). The symbiotic giants in Figure .3 seem form a sequence that is shifted somewhat downwards. In our solution the microturbulence velocity was treated as being free parameter. In all cases we obtained microturbulence values close to 2. Unfortunately abundances of some elements strongly depend on the microturbulence value. Smith et al.

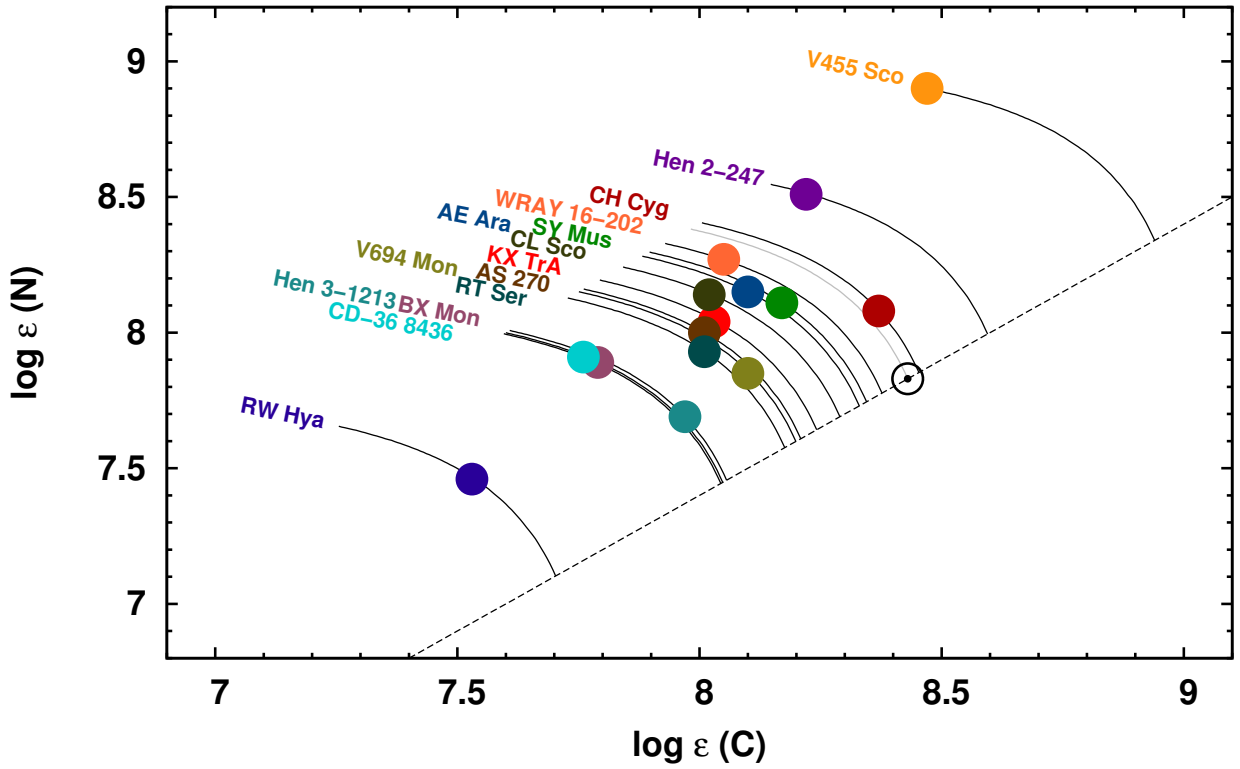

Figure .2: Nitrogen vs. carbon for the symbiotic giants. The dashed line represents scaled solar abundances, [^{12}C/Fe]=0 and [^{14}N/Fe]=0, whereas the solid curves delineate constant ^{12}C+^{14}N, or the so-called 'CN mixing lines'.

(2002) showed that red giants microturbulence is corelated with bolometric magnitudes. We repeated the analysis for BX Mon, AE Ara, KX TrA, and CL Sco adopting the microturbulence values, 2.5, 2.5, 2.5 and 2.3, respectively according to their bolometric magnitudes. The resulting abundances are also shown in Figure .3 by arrows. For BX Mon we also calculated abundances for $\log g = +0.5$ (see Figure .3). The resulting abundances do not show significant differences.

Acknowledgements. This study has been supported in part by the Polish NCN grant No DEC-2011/01/B/ST9/06145. CG has been also financed by the NCN postdoc programme FUGA via grant DEC-2013/08/S/ST9/00581. CG gratefully acknowledges M. R. Schmidt for his valuable comments.

References

Asplund, M., Grevesse, N., Sauval A., & Scott, P. 2009, ARAA, 47, 481

Bessell, M. S., & Brett, J. M. 1988, PASP, 100, 1134

Table .3: Relative [O/Fe] and [Fe/H] abundances.

Object	[O/Fe]	[Fe/H]	Ref.	Object	[O/Fe]	[Fe/H]	Ref.
V694 Mon	+0.13	−0.39	‡	RW Hya	+0.24	−0.76	[1]
CD-36 8436	+0.06	−0.38	‡	SY Mus	+0.05	−0.08	[1]
WRAY 16-202	−0.08	+0.02	‡	BX Mon	+0.02	−0.34	[2]
Hen 2-247	+0.03	+0.12	‡	AE Ara	+0.04	−0.09	[2]
AS 270	−0.06	−0.16	‡	KX TrA	+0.30	−0.33	[2]
RT Ser	+0.21	−0.54	‡	CL Sco	+0.21	−0.29	[2]
V455 Sco	+0.24	+0.30	‡	CH Cyg	+0.07	+0.0	[3]
Hen 3-1213	+0.94	−0.79	‡				

[1] Mikołajewska et al. (2014); [2] Gałan et al. (2014); [3] Schmidt et al. (2006)

Brandt, S. 1998, Data Analysis, Statistical and Comput. Methods, (PWN)

Carlberg, J. K., Majewski, S. R., Patterson, R. J., et al. 2011, ApJ, 732, 39

Fekel, F. C., Hinkle, H. K., Joyce, R. R., et al. 2003, ASPC, 303, 113

Gałan, C., Mikołajewska, J., Hinkle, K. H. 2014, MNRAS, (submitted)

Goorvitch, D. 1994, ApJS, 95, 535

Gustafsson, B., Edvardsson, B., Eriksson, K., et al. 2008, A&A, 486, 951

Hinkle, K. H., Fekel, F. C., Joyce, R. R., et al. 2006. ApJ, 641, 479

Joyce, R. 1992, ASPC, 23, 258

Kucinskas, A., Hauschildt, P. H., Ludwig, H.-G., et al. 2005, A&A, 442, 281

Kupka, F., Piskunov, N., Ryabchikova, T., et al. 1999, A&AS, 138, 119

Kurucz, R. L., http://kurucz.harvard.edu/

Melendez, J., & Barbuy, B. 1999, ApJS, 124, 527

Mikołajewska, J., Gałan, C., Hinkle, K. H., et al. 2014, MNRAS, 440, 3016

Mürset, U., & Schmidt, H. M. 1999, A&ASS, 137, 473

Phillips, J. P. 2007, MNRAS, 376, 1120

Richichi, A., Fabbroni, L., Ragland, S., Scholz, M. 1999, A&A, 344, 511

Schmidt, M. R., Zacs, L., Mikolajewska, J., & Hinkle, K. H. 2006, A&A, 446, 603

Schlafly, E. F., & Finkbeiner, D. P. 2011, ApJ, 737, 103

Smith, V. V., Hinkle, K. H., Cunha, K., et al. 2002, AJ, 124, 3241

van Belle, G. T., Lane, B. F., Thompson, R. R., et al. 1999, AJ, 117, 521

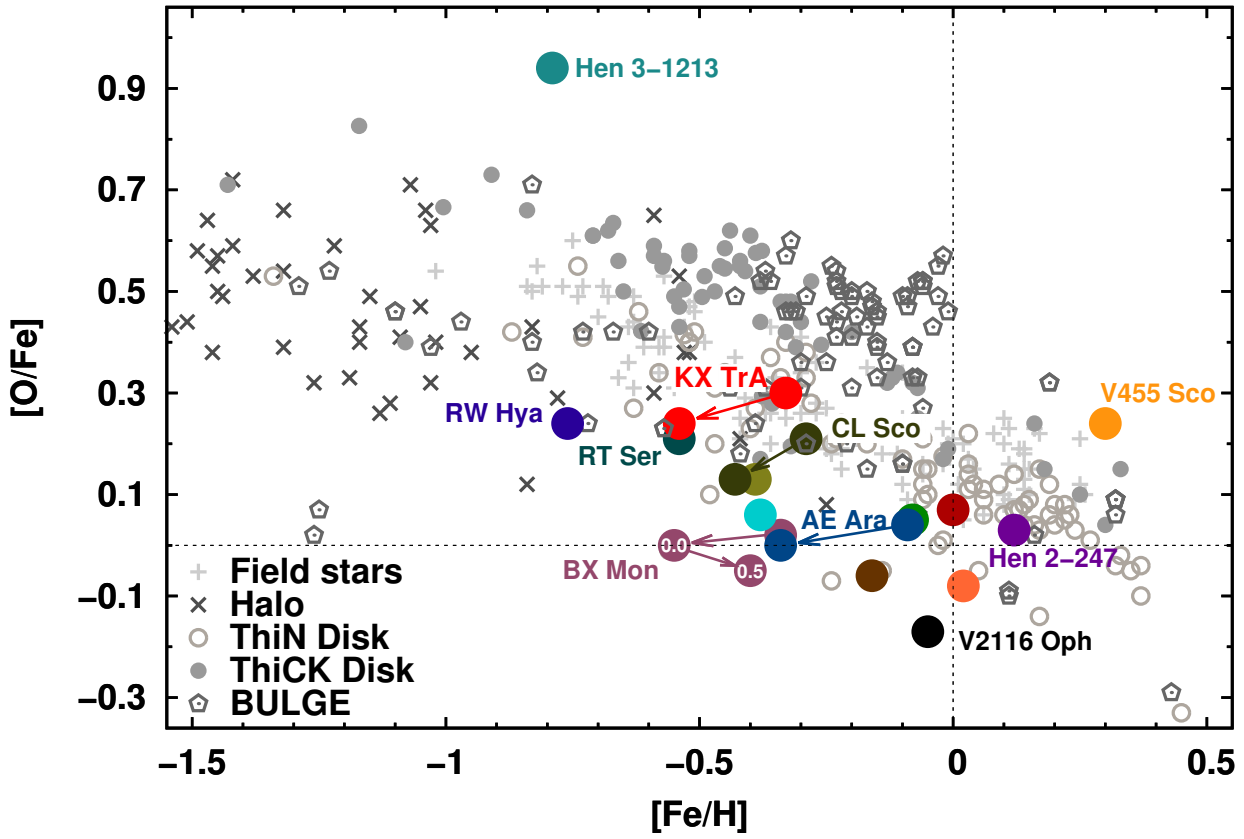

Figure .3: Oxygen relative to iron for various stellar populations with positions of our targets shown with large dots in colors coded in Table .3. Position of V2116 Oph – the symbiotic system with neutron star – according to Hinkle et al. (2006) is also shown.

Our Cool Stars 18 ‘Great Debaters’, Martin Asplund and Marc Pinsonneault .